

Received July 05, 2020; reviewed; accepted August 21, 2020

Study of effective parameters on generating submicron (nano)-bubbles using the hydrodynamic cavitation

Sabereh Nazari ^{1,2}, Sied Ziaedin Shafaei ¹, Ahmad Hassanzadeh ³, Asghar Azizi ⁴, Mahdi Gharabaghi ¹, Rahman Ahmadi ⁵, Behzad Shahbazi ⁶

¹ School of Mining Engineering, College of Engineering, University of Tehran, 1439957131 Tehran, Iran

² School of Resources Engineering, Xi'an University of Architecture and Technology, 710055 Xi'an, China

³ Department of Processing, Helmholtz Institute Freiberg for Resource Technology, Helmholtz-Zentrum Dresden-Rossendorf, Chemnitz Str. 40, 09599 Freiberg, Germany

⁴ Faculty of Mining, Petroleum and Geophysics, Shahrood University of Technology, 3619995161 Shahrood, Iran

⁵ Department of Mining Engineering, Imam Khomeini International University, 3414896818 Qazvin, Iran

⁶ Mining Engineering Department, Tarbiat Modares University, 1411713116 Tehran, Iran

Corresponding author: hassanzadeh@itu.edu.tr, a.hassanzadeh@gmx.de (Ahmad Hassanzadeh)

Abstract: Although submicron (nano)-bubbles (NBs) have been broadly used in the laboratory flotation processes, the role of critical factors in their generation is not adequately explored in the literature. The present study investigates the effect of six key factors on generating submicron-sized bubbles and its application to coarse-sized quartz flotation. Interaction of influential factors is highlighted, which was generally overlooked in previous studies. These parameters i.e. frother type (MIBC and A65), frother dosage (50-130 mg/L), air flow rate (0.1-0.4 L/min), pressure in Venturi tube (250-400 kPa), liquid temperature (22-42 °C) and pH (6-10) were evaluated through software based statistical fractional factorial design. The size distribution of NBs produced by the principle of hydrodynamic cavitation was measured using a laser particle size analyzer (LPSA), and Sauter mean bubble diameter (d_{32}) was considered as the response of experimental design. Batch flotation experiments were performed with and without the A65 and MIBC-NBs. The results of experimental design showed that relative intensity of the main factors followed the order of air flow rate > temperature > frother type as the most effective parameters on the bubble size. It was revealed that the lowest air flow rate (0.1 L/min) produced the smallest bubbles. Meanwhile, the d_{32} decreased as the liquid temperature increased, and the bubble size strongly was related to the frother type and its concentration. Indeed, with changing frother from MIBC to A65, the reduction in mean bubble size was two-fold. Interaction of frother type with its dosage, air flow rate and pressure were statistically recognized significant on the mean bubble size, which was confirmed by p-values. Finally, flotation recovery of quartz particles improved *ca.* 22% in the presence of NBs compared to the conventional flotation.

Keywords: coarse quartz particles, bulk nanobubbles (NBs), fractional factorial design, frother type, temperature

1. Introduction

Nowadays, submicron-sized bubbles *a.k.a.* nano-bubbles (NBs) or ultrafine bubbles have found many applications in various industries. Although the title of these bubbles has been remained an argument in the literature, the term nanobubble is broadly applied in many reports (Nazari and Hassanzadeh, 2020), which is henceforward used in the present paper. They are benefited in the medical (Zhang et al., 2020) agriculture (Neethirajan et al., 2011), food (Kumar et al., 2009), water treatment (Agarwal et al., 2011; Azevedo et al., 2017), and mineral processing industries (Calgaroto et al., 2015; Nazari et al., 2018; Nazari et al., 2019; Tao and Sobhy, 2019). Bulk and surface NBs are typically negatively charged,

have high stability and longevity retention time, along with high surface area per volume (Yekeen et al., 2017). These properties allow them to be desirably used in froth flotation processes (Hassanzadeh et al., 2020), although the NBs demonstrate low buoyancy force and move slowly to the froth zone. Several researchers have shown that NBs produced by hydrodynamic cavitation (HC), selectively alter mineral surface properties in the case of hydrophobic particles (Hampton and Nguyen, 2010; Fan et al., 2012), increase flotation kinetics rate (Nazari et al., 2019), enhance the contact angle of the solids and the particle-bubble attachment force (Fan et al., 2010; Fan et al., 2012; Nazari et al., 2019). The capillary bridge generated from the coalescence of NBs provides a high probability of particle-bubble attachment efficiency. They remove oxidation layers from the particle surfaces and reduce reagent consumption (Zhou et al., 1997; Fan and Tao, 2008).

NBs are generated by various methods including ultrasonic (Farmer et al., 2000; Kim et al., 2000), water solvent mixing (Lou et al., 2000; Paxton et al., 2004), microfluids (Nirmalkar et al., 2018), electrolysis (Chen et al., 2015), pressure reduction (Ahmadi et al., 2014; Nazari et al., 2019) and temperature variation (Zhang et al., 2007). Many researchers have investigated the use of NBs in the froth flotation. Li et al. (2020) studied the entrainment behavior of kaolinite in nanobubble- assisted flotation. They disclosed that bulk NBs increased the kaolinite entrainment. Fan et al. (2010) indicated that the recoverability of coal and phosphate particles improved in the presence of them. Nazari et al. (2019) investigated the construction of NB generator and their application to the flotation of coarse quartz particles. They reported an increase of 21% in the recovery of quartz particles. Xiao et al. (2019) addressed the effect of sodium oleate on the adsorption morphology and mechanism of nanobubbles on the mica surface. The results indicated that the nanobubbles are highly selective for the activation sites on the mineral surface in the adsorption mode. Other than fine (<20 μm) and coarse-sized (>100 μm) particles, most recently Rulyov et al. (2020) examined the role of microbubbles produced by MBGen-0.012 generator in cetyltrimethylammonium bromide (CTAB, $\text{C}_{19}\text{H}_{42}\text{BrN}$) solution in flotation efficiency of medium size (50–80 μm) glass beads (ballotini). They reported a significant increase in the flotation rate and the ultimate recovery using combined macro- and micro-bubbles.

A common method to produce ultrafine bubbles in the flotation system is the HC. This action occurs when the liquid pressure with a sudden increase in flow velocity reaches below a critical amount (Brennen, 2014; Nazari et al., 2018). Fig. 1 shows the generation of NBs by changing process factors.

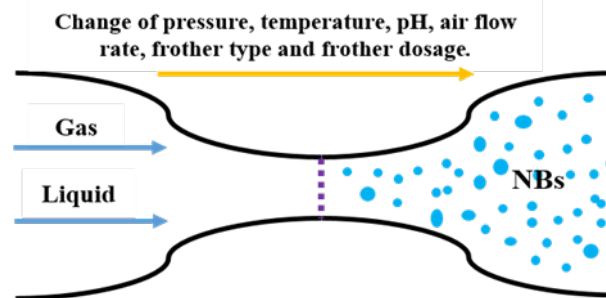


Fig. 1. Schematic overview of nanobubble generation by the hydrodynamic cavitation

Although the application of NBs in froth flotation systems is extensively reported in the literature, there is little technical information supporting the role of effective parameters in their properties (size distribution, surface charge and stability). In this regard, Meegoda et al. (2018) addressed the stability and surface charge characteristics of hydrodynamically cavaeted bubbles by varying gas nature (air, oxygen, nitrogen, and ozone), salt concentration (0.001, 0.01, 0.1, and 1 M solutions), pH level (4, 7, and 10), and temperature of the solution (15, 20, and 30 $^{\circ}\text{C}$). It was found that small-sized bubbles were generated under high solution pH values, and bubbles were bigger and unstable in acidic solutions. These results supported the hypothesis that the amount of OH^- ions on the surface governed the stability of NBs. Higher pH levels with a significant concentration of OH^- ions generated smaller and stable bubbles with higher zeta potential values. The solution temperature showed no significant change in the bubble size. Following this, Azevedo et al. (2016) generated NBs by decreasing the pressure of deionized water and characterized the mean size and concentration of the bubbles via nanoparticle-tracking analysis. They found that the bubbles became smaller and more electronegative when the

medium pH changed from 3 to 8; the mean diameter halved from 500 to 250 nm, and the zeta potential reduced by approximately 40 mv units. Most recently, Nazari and Hassanzadeh (2020) showed the role of three commonly used frothers (MIBC, pine oil and A65) and one collector (DDA) in the stability of the bubbles. It was found that DDA-NBs were the most stable ones followed by pine oil-, MIBC- and A65-NBs, which was related to its frothability property, longer hydrocarbon chain and OH- function. Also, Pourkarimi et al. (2017) studied the median size and volume of NBs generated through the HC by varying the frother type and its dosage, pressure in Venturi tube, gas types, air flow rate, pH, temperature and diameter of the Venturi tube by means of central composite design (CCD). The bigger diameter of Venturi tube and higher value of the pressure led to larger and smaller bubble sizes, respectively. One principle issue concerning these studies is that none of them considered the interaction of the influential factors. For example, by changing the temperature, rate of dissolved gas and even pH varies inherently, which have been entirely overlooked. Therefore, it is un-preferential to utilize one-factor-at-a-time (OFAT) method because of ignoring the interaction effect of parameters (Hassanzadeh et al., 2019). Nowadays, it is known that design of experiment (DOE) combined with statistical modelling, is a powerful, economical and practical technique to study the multivariable systems and to analyze the processes, especially in the mineral processing industries. This methodology quantifies the relationship between the controllable input factors and the obtained outputs even in the presence of complex interactions (Azizi et al., 2020).

In this study, the impact of six key factors (frother type, frother dosage, air flow rate, pressure in the Venturi tube, liquid temperature and pH) and interaction of the effective factors on generating NBs were investigated by a fractional factorial design. This design offers a powerful evaluation capability for determining the most significant influential parameters. Further, flotation experiments of coarse quartz particles were undertaken with and without the NBs as a proof of concept.

2. Materials and methods

2.1. Materials

Coarse quartz sample (high purity of >99%), taken from Techno Silis Inc. (Hamedan, Iran) with the size of -425+106 μm and specific gravity of 2.65 g/cm^3 was used for flotation experiments. Jaw and roll crushers were applied to reduce the particle size down to approximately 100 μm . Then, the quartz particles were sieved at -425+100 μm range and prepared for the flotation experiments. Table 1 presents the particle size distribution obtained by sieving process.

This size fraction was opted based on the results of our previous work (Nazari et al., 2019). Table 2 exhibits the sample characteristics using Philips PW 2404 X-ray fluorescence spectrometer (XRF).

Dodecyl amine (99%, $\text{CH}_3(\text{CH}_2)_{10}\text{CH}_2\text{NH}_2$) with a dosage of 50 mg/L was used as a collector. MIBC (98% purity, methyl isobutyl carbinol, $\text{C}_6\text{H}_{14}\text{O}$) and A65 (98% purity, polypropylene glycol $\text{C}_6\text{H}_{14}\text{O}_3$) with the concentration of 50 mg/L were used as a frother for flotation experiments. Also, MIBC and A65 with a concentration of 50 to 130 mg/L were used for producing NBs. Furthermore, pH was adjusted employed hydrochloric acid (HCl, 37%, Merck GmbH) and sodium hydroxide, NaOH (Merck GmbH).

Table 1. The particle size distribution of coarse quartz samples

Sieve size (μm)	Weight (g)	Cumulative passing (%)
+425	0.00	100.0
-425+300	41.7	70.6
-300+212	36.6	44.5
-212+106	62.7	0.00
-106	0.00	0.00

Table 2. The results of XRF analysis for the quartz particles

Component	SiO_2	Al_2O_3	CaO	Na_2O	Fe_2O_3	K_2O	MgO	P_2O_5	SO_3	L.O.I*
Content (wt%)	99.901	0.011	0.010	0.007	0.010	0.007	0.004	0.005	0.008	0.037

* L.O.I is the loss on ignition

2.2. Contact angle measurement

Contact angle measurement of quartz powder was conducted by Washburn method. The Lauda Tensiometer (TE3, LAUDA, Germany) was applied to quantify wetting behavior of the whole surface. The contact angle was measured by means of the precise adjustment of the immersion/receding rate and micrometer-accurate measurement of the immersion dept. Its value for the quartz sample after flotation tests was achieved 89.70°.

2.3. Generating submicron(nano) bubbles

The NBs were generated using the HC concept via a laboratory generator designed and developed at the Iranian Mineral Processing Research Center (IMPRC) (Fig. 2). Production of NBs was conducted at 22-42 °C using tap water. Basically, a great amount of water was stocked while its characteristics such as temperature, conductivity and pH were monitored in daily routine. We utilized the stored water in all the experimental works to avoid its contamination and keeping its effectiveness on the results constant. To analyze water properties, the inductively coupled plasma-mass spectrometry (ICP-MS, Perkin-Elmer ICP/6500, USA) was used. Table 3 represents its chemical characteristics. Moreover, air flow rate was adjusted at 0.1 to 0.4 L/min and the pressure was considered 250 to 400 kPa.

Table 3. The concentration of target elements in tap water

Element	Na	Ca	Mg	K	Sr	Ba	B	Si	As	Pb	Zn	Mn	Cu	Cr	Cd
ICP (ppm)	250	50	30	8	0.2	0.1	1	6	<0.05	<0.05	<0.05	<0.05	<0.05	<0.05	<0.05

The NB generator was consisted four major parts: i) air (gas) entry, ii) application of pressure on the air/water mixture, iii) the zone of reduction or pressure drop and iv) the part of release of the dissolved air. The purpose of air entry was to increase air dissolution into water to increase the cavitation efficiency and produce NBs (Ahmadi et al., 2014; Nazari et al., 2019).

To generate NBs, water and a specific amount of frother were initially mixed. The prepared solution was pumped through a centrifugal pump to a Venturi tube with a specific dimension, and later, as shown in Fig. 2 filtered air was injected into the solution upstream of the pump. The pump was free of leaks and corrosion-resistant. With the use of two static mixers in the down-stream and up-stream of the pump, the dissolution of air at the entrance of Venturi tube was increased. Depressurization of the air-saturated water led to the generation of the bulk NBs. Bubble sizes were measured by laser particle size analyzer (Master size 2000, Malvern, UK) as a widely utilized approach in the literature (Ahmadi et al., 2014; Pourkarimi et al., 2017). The average diameter of d_{32} (Sauter mean bubble diameter) was used to determine the mean bubble sizes, which is accepted as a well-known indicator (Shahbazi, 2015; Kracht and Moraga, 2016) and formulated as $d_{32} = \frac{\sum d_i^3}{\sum d_i^2}$. The d_{32} is the volume-to-surface mean bubble diameter, produces the same surface area to volume ratio as the bubble size distribution (BSD); it is usually applied to determine the mean bubble size in analysis of flotation systems. The device was regulated in a way to operate quintuple to meet desirable reproducibilities in the sense of measuring d_{32} s. Fig. 3 shows the BSDs of NBs under the identical operating conditions.

2.4. Design of experiments

Design expert software (Demo v.7.0.0 State-Ease, Inc., Minneapolis, MN, USA), randomized fractional factorial design (2^{6-2}), was used to investigate six effective parameters (frother type, frother dosage, air flow rate, pressure drop in Venturi tube, liquid temperature and pH) on the bubble size. This specific design permits to estimate all main effects and interaction of parameters. By introducing the data to the software, 24 set of tests ($N = 2^{(6-2)} + 8 = 24$) were undertaken, including eight central points, while the desired response was the bubble size. Table 4 shows the experimental design, factors and their levels. Meanwhile, experiments were repeated twice (except for central tests), and results were averaged. Reproducibility of the experiments is performed by the the central tests. For instance, central tests for frother of A65 are run 18 ($d_{32}= 307$ nm), run 20 ($d_{32}= 303$ nm), run 22 ($d_{32}= 294$ nm) and run 24 ($d_{32}= 288$

nm). As considered, the changes for mean bubble size is very low under identical experimental conditions including pH=8, frother dosage= 90 mg/L, air flow rate= 0.25 (L/min); temperature= 32 °C, pressure= 325 kPa. In other words, these repetitions give an average of 298 ± 8.4 nm in 95% confidence level. After conducting all the experiments, the average diameter of NBs so-called Sauter mean bubble diameter (Hassanzadeh et al., 2017) was obtained as shown in Table 4. It needs to be pointed out that the range of factors studied was selected based on a series of primary experiments and previous works published in this field (Pourkarimi et al., 2017; Nazari et al., 2018; Nazari et al., 2019; Nazari and Hassanzadeh, 2020).

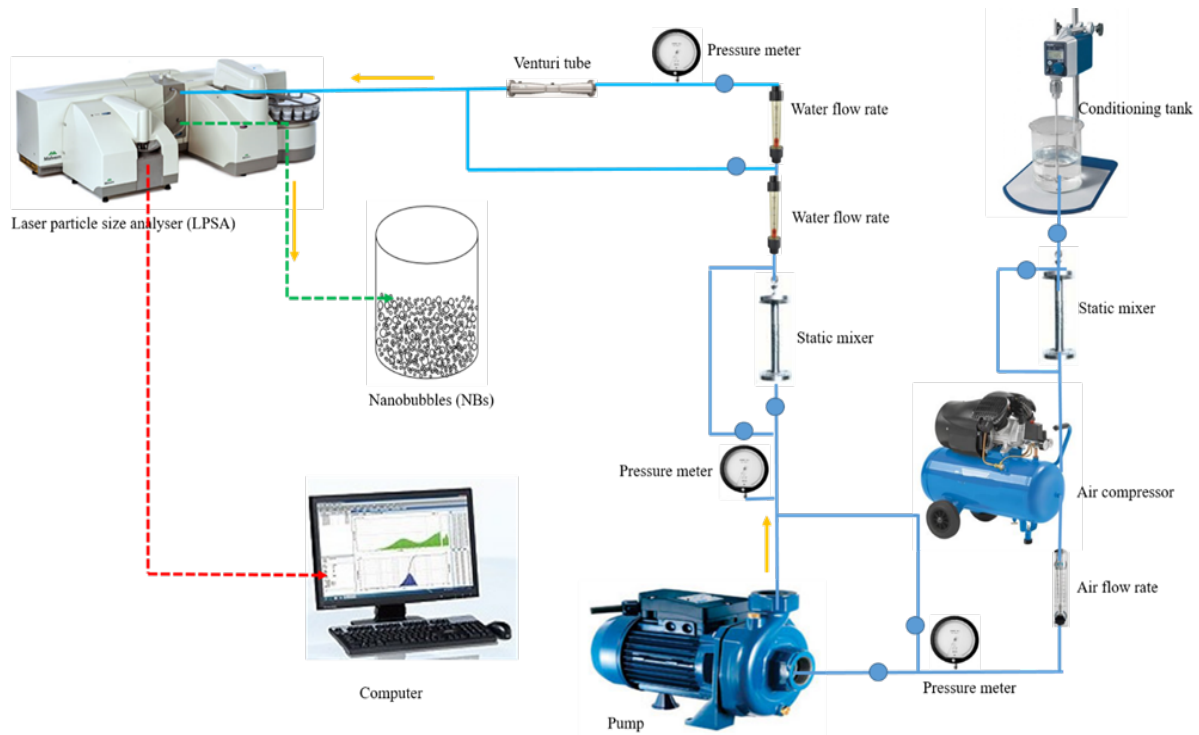


Fig. 2. Schematic view of the laboratory set-up system for NB generation (Nazari et al., 2019)

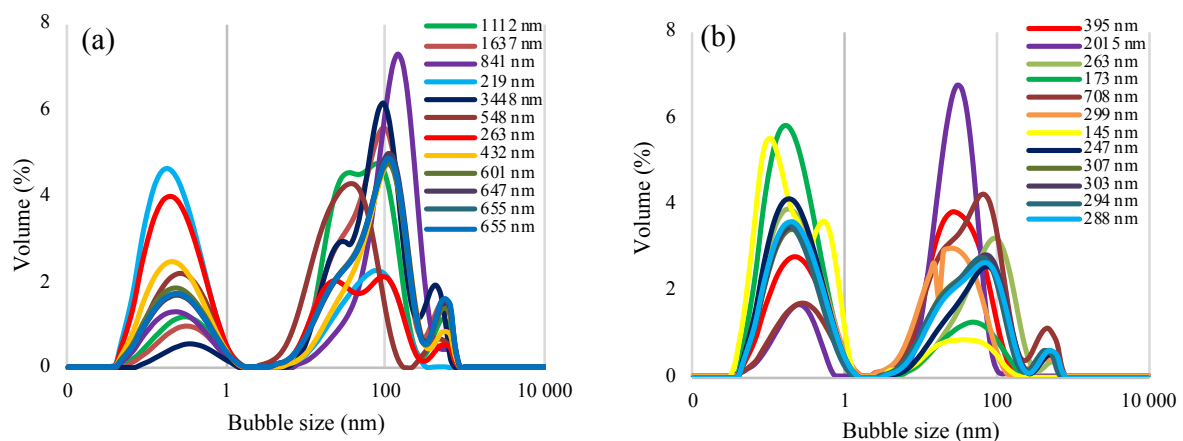


Fig. 3. Bubble size distribution of generated NBs by means of a) MIBC and b) A65 for different mean bubble sizes

2.5. Flotation experiments

The experimental work was performed in a 1 L laboratory mechanical flotation cell, 10% (w/w) solid content (141 g initial mass of quartz) and at an air flow rate of 30 L/h. The cell was agitated with the rates of 900 and 1100 rpm in case of with and without NBs, respectively. The collector and frother were conditioned for 2 and 1 min, respectively. Frother was added through two ways:

Table 4. Proposed experiments with design expert software with fractional factorial design

Run No.	Factor A: Frother type	Factor B: Frother dosage (mg/L)	Factor C: Air flow rate (L/min)	Factor D: Pressure (kPa)	Factor E: pH	Factor F: Temperature (°C)	Response: Bubble size (nm)
1	MIBC	50	0.1	250	6	22	1112
2	A65	50	0.1	250	10	22	395
3	MIBC	130	0.1	250	10	42	1637
4	A65	130	0.1	250	6	42	2015
5	MIBC	50	0.4	250	10	42	841
6	A65	50	0.4	250	6	42	263
7	MIBC	130	0.4	250	6	22	219
8	A65	130	0.4	250	10	22	173
9	MIBC	50	0.1	400	6	42	3448
10	A65	50	0.1	400	10	42	708
11	MIBC	130	0.1	400	10	22	548
12	A65	130	0.1	400	6	22	299
13	MIBC	50	0.4	400	10	22	263
14	A65	50	0.4	400	6	22	145
15	MIBC	130	0.4	400	6	42	432
16	A65	130	0.4	400	10	42	247
17	MIBC	90	0.25	325	8	32	601
18	A65	90	0.25	325	8	32	307
19	MIBC	90	0.25	325	8	32	647
20	A65	90	0.25	325	8	32	303
21	MIBC	90	0.25	325	8	32	655
22	A65	90	0.25	325	8	32	294
23	MIBC	90	0.25	325	8	32	655
24	A65	90	0.25	325	8	32	288

I. without NBs, the frother was introduced directly into the flotation cell.

II. with NBs, 77% of the frother (770 mL) was introduced into the cell in the form of NBs and after 30 s, the residual frother (23%, 230 mL) was directly added. Also, the NBs were entered to the flotation cell with the time span of 12 s. It is worth mentioning that the frother consumptions in Venturi tube at the air flow rate of 0.4, 0.25 and 0.1 L/min were 2.57, 1.61 and 0.64 mg/L, respectively.

Ultimately, flotation was performed with opening the air flow rate. Concentrates were collected after 2.5 minutes. The quartz recovery was calculated based on the following Equation:

$$R = \frac{C}{F} \times 100 \quad (1)$$

where R (%), C (g) and F (g) are the recovery, concentrate and feed masses, respectively.

3. Results and discussion

3.1. Estimation of mean bubble size

Statistical analysis of the results obtained from 24 experiments was performed to show if the effect of process parameters was statistically significant. This was implemented through the analysis of variance (ANOVA) as a commonly used statistical technique (Rath et al., 2013; Hassanzadeh and Karakas, 2017) to demonstrate the effect of different factors by the total variation into its appropriate components. The result of ANOVA analysis for the bubble size was shown in Table A1 in the appendix. Also, a mathematical function for statistical analysis of the results was presented (Equation A1).

In that Equation, F-value is a criterion to compare the model with residual variances. The ratio will be close to 1 if the variances are close to the same. The F-values of the proposed model and also the very low probability of 0.0001 indicate the significance of the model. P-values less than 0.05 indicate that the importance of model parameters is significant within the 95% confidence interval. These findings can also be affirmed from the graphs illustrated in Fig. 4, which applies to further check the adequacy of the

model. Figure 4 indicates the residual normal probability (Fig. 4a), predicted values versus actual data (Fig. 4b), Box-Cox plot which is a tool to estimate the transfer power of the model (Fig. 4c) and internally studentized residuals values amongst predicted values (Fig. 4d). As seen, the residual values (the deviation between the predicted and actual values) follow the normal distribution well. Additionally, the R-squared (R^2) value of 0.9986 is indicative of the high accuracy of the proposed model to foreseeing the responses.

In addition, the behavior of influential factors was assessed by the perturbation plots, as shown in Fig 5. This graph was obtained by Design expert software in the state of without transeformation, and it helps us to compare the effect of all the factors at a particular point in the design space. A steep slope or curvature in a factor indicates that the dissolution rate is sensitive to that factor (Katal et al., 2020). In this plot, factors are studied with their codified values for uniform comparison according to the following equation (Azizi et al., 2020):

$$x_i = \frac{X_i - X_0}{\Delta X} \quad (2)$$

where x_i implies the dimensionless coded value of the i^{th} factor, X_i denotes the actual value of the factor, X_0 represents the value of X_i at the center point and ΔX is the step change value.

It can be observed from Fig. 5 that, to produce NBs by means of the HC, three factors including air flow rate, temperature and frother type were significant model terms. Other parameters had less effect on NBs generation. Consequently, according to the results, the smaller bubbles could be achieved using a high air flow rate, a low temperature and A65 frother at a low concentration. In general, it is found that the significance of the essential terms is in the order of air flow rate > temperature > frother type > pressure > frother dosage > pH. More detailed discussions in this regard can be found in section 3.2.

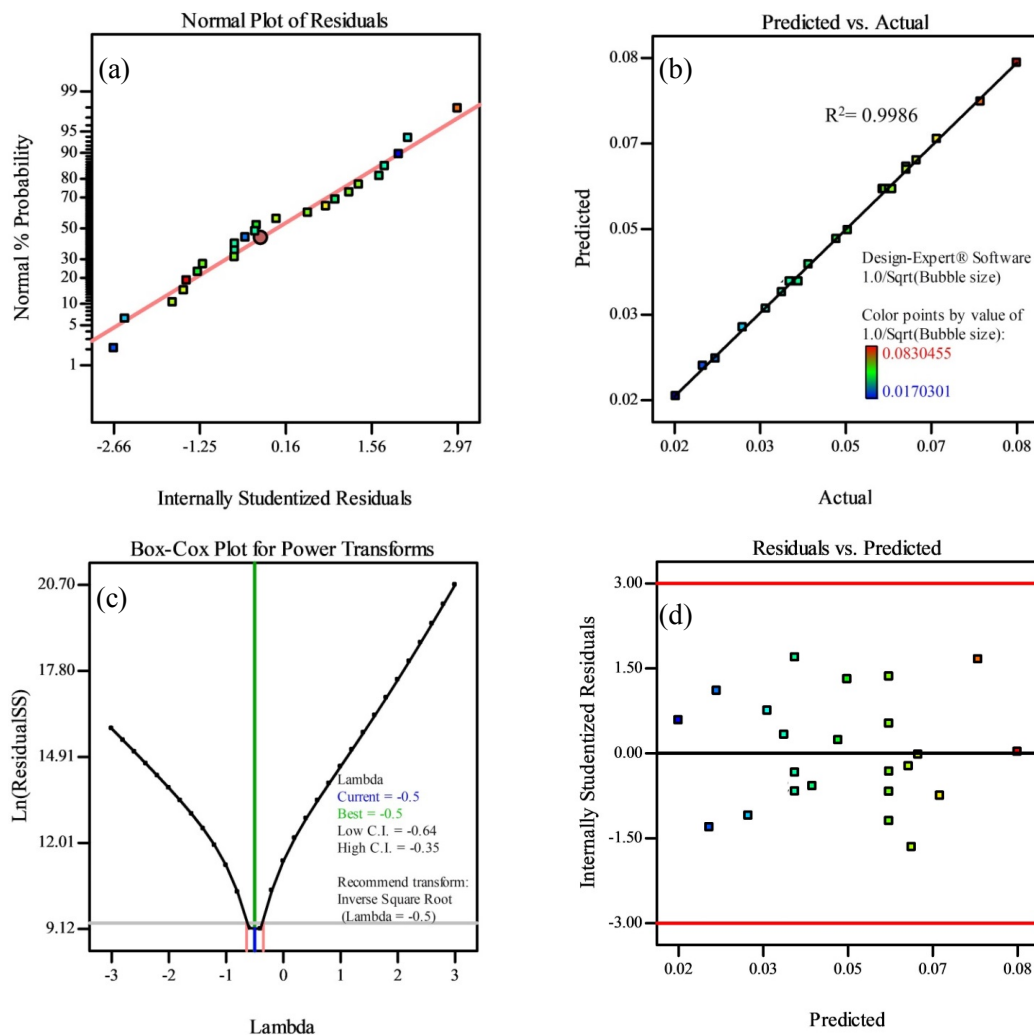


Fig. 4. Statistical diagnostics of model

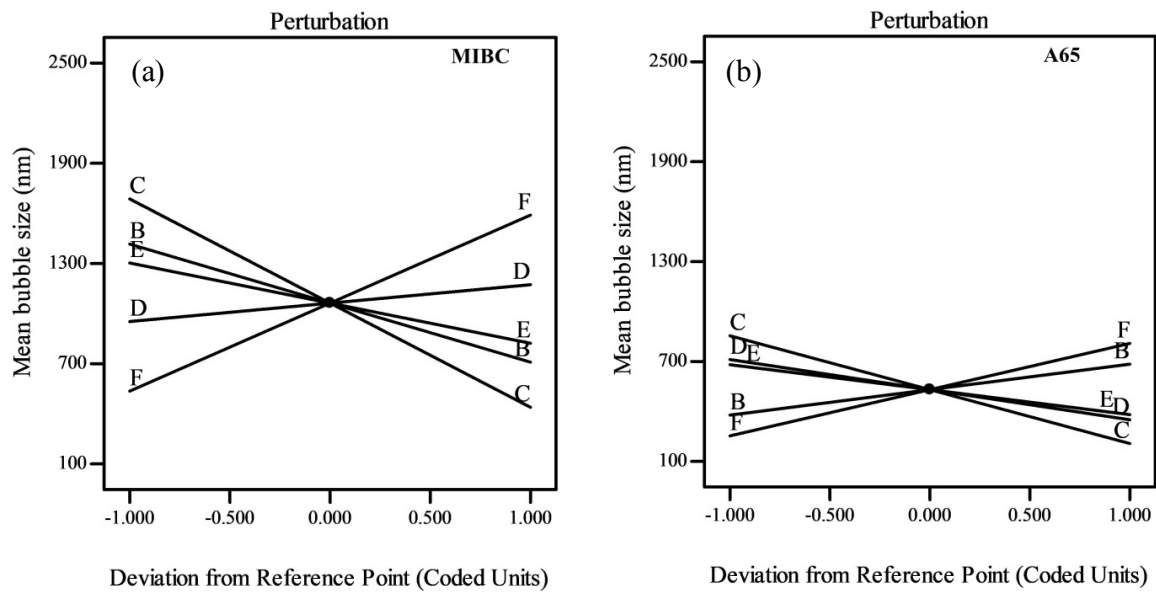


Fig. 5. Perturbation plot showing the relative significance of factors for frothers of (a) MIBC and (b) A65 based on coded values

3.2. Effective parameters

3.2.1. Frother type and its concentration

One of the most effective parameters on the bubble diameter and bubble velocity is frother type (Hassanzadeh et al., 2018). The size of ultrafine bubbles significantly influences the effectiveness of their application and depends on the concentration of a collector/frother used for their generation (Rulyov et al. 2020). Fig. 6a displays that A65 produces relatively smaller and reasonably uniform bubbles than MIBC. This is also confirmed by the data presented in Table 4 (runs 17-24) and Fig. 7. It is observed from Fig. 7a that the mean bubble size reduces from about 601 nm to 312 nm with the change in frother type from MIBC to A65. Meanwhile, considering Table 4, it is found that the decrement in bubble size was doubled with selecting A65 frother. Additionally, it can be seen from Fig. 7b that by increasing the dosage of MIBC from 50 to 130 mg/L under conditions including 8 pH, 90 mg/L frother dosage, 0.25 L/min air flow rate, 32 °C temperature and 325 kPa pressure, the bubble size falls from about 780 nm to 477 nm. However, for A65, the rise of concentration has no positive effect on the mean bubble size in the range investigated (Fig. 7c).

As seen in Table 4, under a constant experimental condition (air flow rate=0.25 L/min, pressure=325 kPa, pH=8 and temperature=32 °C) by only varying the frother type at the constant dosage of 90 mg/L, the mean bubble sizes for MIBC and A65 were obtained as 639 ± 25 nm (average of runs 17, 19, 21 and 23) and 298 ± 8 nm (average of runs 18, 20, 22 and 24), respectively. In addition to the bubble size, volumetric concentration and stability of generated NBs via these surfactants is another crucial factor, which we discussed them in detail in our previous work (Nazari and Hassanzadeh, 2020). It was found that they produce NBs with somewhat similar stabilities that MIBC-NBs were slightly more stable. The reason for such phenomenon can be argued from different perspectives such as chemical functionality, ionic strength, adsorption mechanism and solubility (Ahmadi and Khodadadi Darban, 2013; Pourkarimi et al., 2017). Further observations regarding their surface properties and surface tension measurements can be helpful for a profound understanding of this concept.

Table 5 comparatively represents the chemical structure and other related characteristics of both frothers. As seen, the molecular weight of A65 is relatively higher than MIBC leading to an excessive change of the surface tension and possibly intensive zeta potential of the bubbles. Guven et al., 2020 reported that CCC of polypropylene glycol and MIBC as 3 and 10 ppm for conventional-sized bubbles, respectively, which is relatively below the results reported in Table 5. This discrepancy can be related to the variant measurement methods. They indicated that polypropylene glycol is more surface-active agent than the rest of surfactants tested, including MIBC, which is in line with our conclusion regarding

their effectiveness on the water-gas interface. In this scope, Pourkarimi et al. (2017) also examined five different frothers at 100 mg/dm³ *i.e.* MIBC, Pine 90, Flo-Y-S (mixed fatty acid), propylene glycol (A65), PEB 70 and Apirole. They sorted them based on the obtained d_{50} (nm) of the created bubbles with an identical generation method as Pine 90<Apirole<A65<MIBC<PEB 70, however, the reason of such behavior was overlooked.

Table 5. Relevant properties of the studied frothers

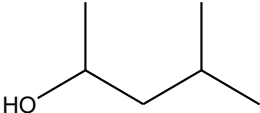
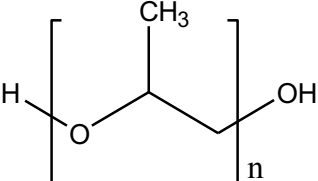
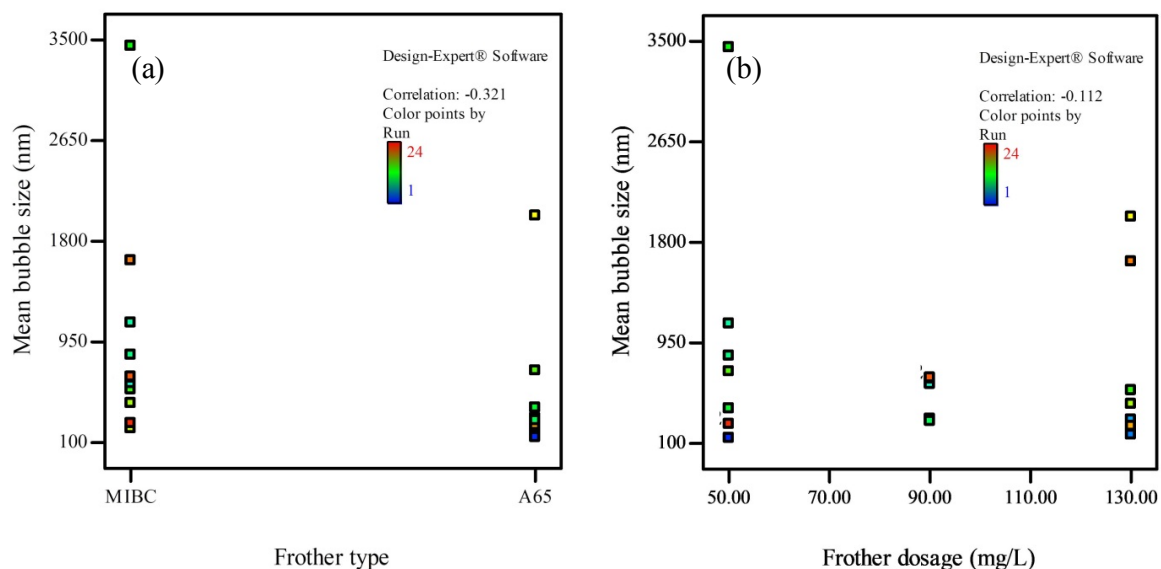
Frother	Structure	Molecular weight (g/mol)	Surface tension (mN/m)	Solubility (g/L)	Critical Coalescence Concentration (ppm)
MIBC		100.16	22.70	17.00	20.00
A65		134.17	36.51	Miscible (completely)	25.00

Fig. 6b demonstrates the role of frother dosage (50, 90 and 130 mg/L) on the d_{32} based on the experimental runs. As seen, there is an optimum frother dosage (90 mg/L) where the generated bubbles have shown slightly smaller quantities with low variance. Nevertheless, it should be noted that the interactive effect of frother type and its concentrate can be an influential factor for this trend. Interestingly, neither Fan et al. (2010) nor Meegoda et al. (2018) considered the interaction of frother type and its dosage on the Sauter number and bubble zeta potential. According to Equation B1, it is clear that the interaction of frother types and their dosage negatively affects d_{32} .

Fig. 6. The role of a) frother type and b) frother dosage on d_{32} based on runs

3.2.2. Air flow rate

Air flow rate has a vital impact on the occurrence of cavitation. Bubble average diameter was decreased with developing air flow rate from 0.1 to 0.4 L/min (Fig. 8a). It can also be observed from Fig. 8b and

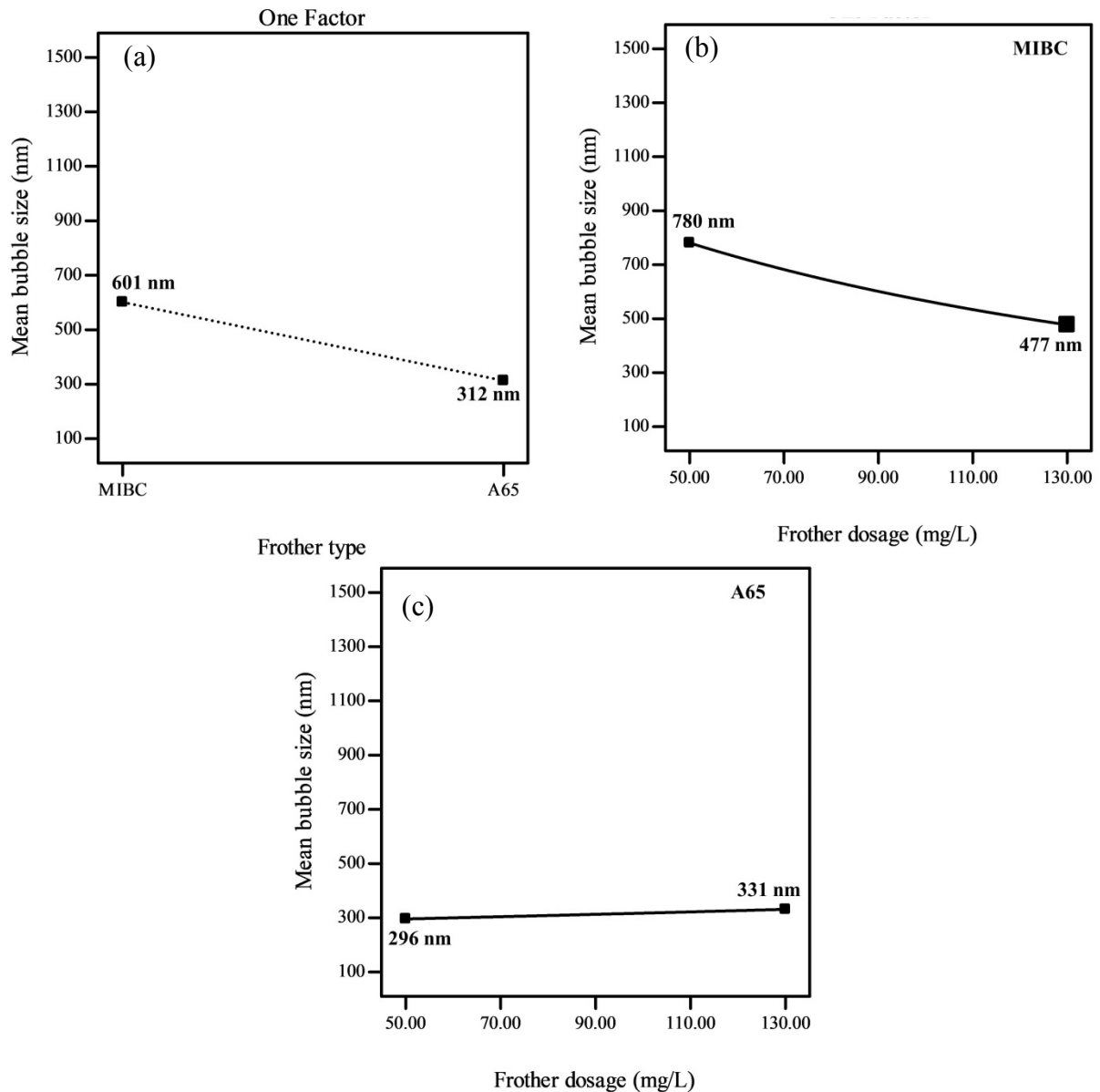


Fig. 7. The effect of a) frother type and b) MIBC dosage and c) A65 dosage on d_{32} based on model predictions (prediction conditions: pH= 8, air flow rate= 0.25 L/min, temperature= 32 °C, pressure= 325 kPa)

Fig. 8c that with changing air flow rate in this range, the mean bubble size sharply reduces from 629 to 243 nm (Fig. 8b) and from 432 to 168 nm (Fig. 8c) when MIBC and A65 are used as a frother, respectively. It is noteworthy that these results were obtained when other factors were kept constant at 8 pH, 90 mg/L frother dosage, 32°C temperature and 325 kPa pressure. The decreased size of NBs with increasing the air flow rate was attributed to the increasing dissolved gas magnitude. The gas solubility affects the nucleation process of NBs. So, gas molecules with high solubility can be closer to each other in solution. Therefore, the bubble nucleation was easily happened, and smaller NBs were formed due to the more nucleation sites. Furthermore, it was shown previously that the gradient of dissolved air decreased at bubble-water interface leading to remaining the air and the pressure inside NBs constant (Zhang et al., 2005; Hamamoto et al., 2008). Consequently, the bubble stabilities increased and also caused the bubble size to become smaller. Ahmadi and Khodadadi Darban (2013) as well as Pourkarimi et al. (2017) have investigated the effect of air flow rate on the NBs size. They found that bubble sizes reduced with enhancing the air flow rate at the constant temperature. Also, Arias et al. (2009) have demonstrated that bubble size was increasing as a function of the gas flow rate, which was in contradictory of the observation of Duong et al. (2019). Regarding the effect of changes in liquid flow

rates, the size of bubbles reduced as air flow rate increased (Arias et al., 2009). Also, Meegoda et al. (2018) proved that the gas pressure and gas flow rate were major contributors to the bubble size. This was relatively supported by our findings that air flow rate is given as one of the crucial factors; however, the influence of pressure drop is not significantly effective on the d_{32} at the studied ranges.

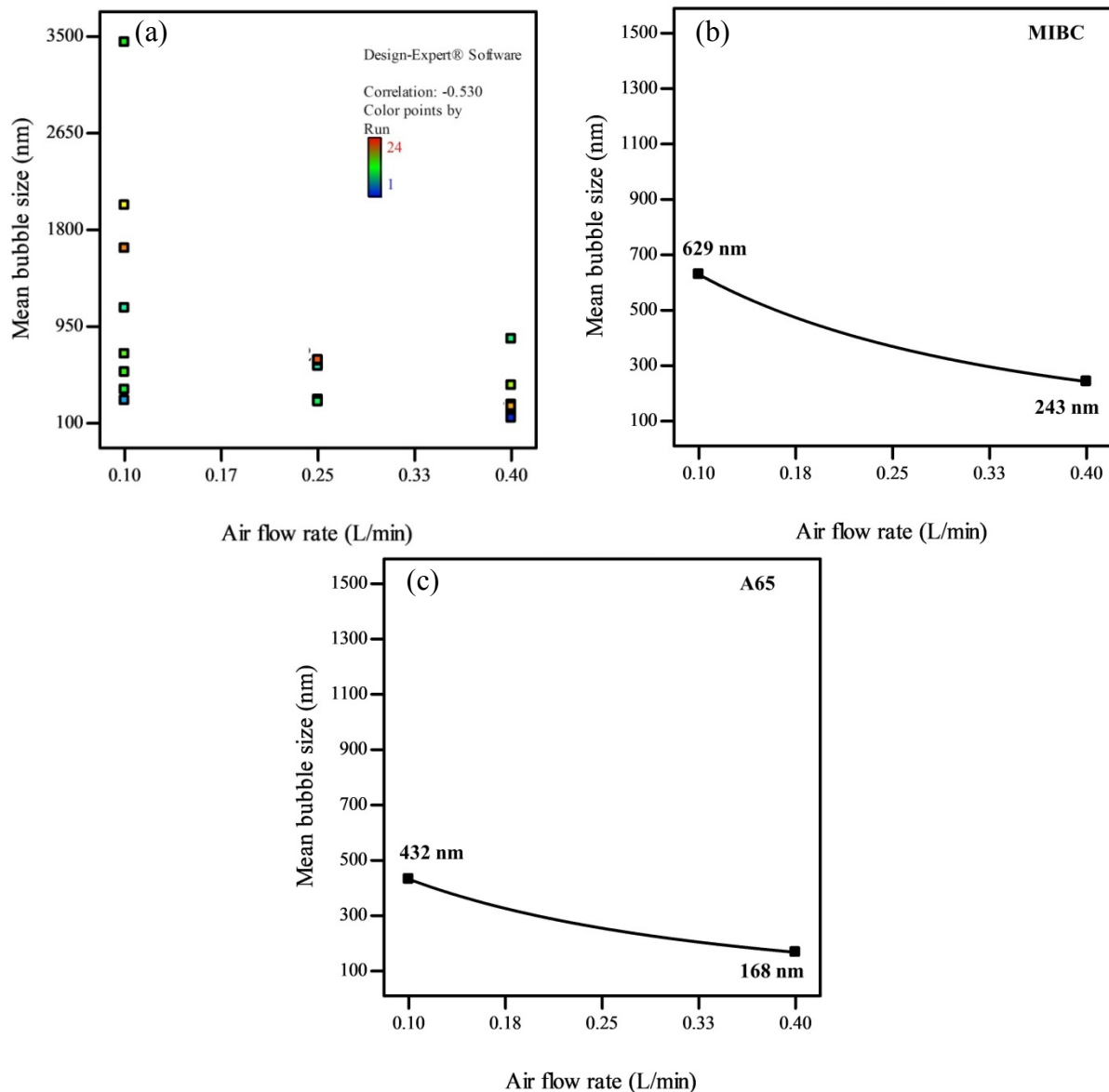


Fig. 8. The role of air flow rate on mean bubble size based on runs (a) and model predictions: (b) MIBC and (c) A65 (prediction conditions: pH= 8, frother dosage= 90 mg/L, temperature= 32 °C, pressure= 325 kPa)

3.2.3. Temperature

Fig. 9 shows the impact of liquid temperature as one of the critical factors on the mean bubble size. As seen, by increasing the temperature from 22 °C to 42 °C, the bubble size rises up. As can be observed from model predictions (Fig. 9b), the mean bubble size strongly enhances from 334 nm to 737 nm when MIBC is used as a frother at pH of 8, frother dosage of 130 mg/L, air flow rate of 0.25 L/min, and pressure of 325 kPa. Whereas, under these conditions for A65 frother, the mean bubble size increased from 230 nm to 518 nm. The reason for this can be owing to the fact that the temperature causes the formation of a bubble at a lower liquid flow velocity in the Venturi tube, which is in relation to enhancement of water vapour pressure and, consequently, a reduction in the number of cavitation. Also, an increase in the liquid temperature leads to an improvement of the bubble density. The temperature impact on the bubble size has remained an argument in the literature yet. We presume that

temperature dependence of the gas solubility in water can be a possible reason while a slight gas solubility variation in water might cause a considerable impact on the bubble size. In this regard, Fan et al. (2012) investigated the interlinked effect of slurry temperature and dissolved oxygen gas content on the median size of the NBs generated by the hydrodynamic cavitation. It was pointed out that the d_{32} considerably increased with increasing the temperature (25-28 °C) at each level of $O_{2(g)}$ concentration (7.3-8.8 ppm). This conclusion generally fits our finding, where we explore it even for higher temperatures (>28 °C). Following this, Zhang et al. (2005) observed surface NBs generated by water-ethanol exchange method on mica by tapping mode in AFM. They found that the temperature not only significantly affects the NB size, but it impacts its shape by dominantly deforming bubble lateral size. Also, the bubbles detected in 37 °C were larger than 32 °C and 42 °C. Considering the previous outcomes and the results given in Figure 9, we believe that the interconnected effect of solubility, dissolved oxygen rate and potential charge of bubbles all together lead to observe larger mean bubbles in higher temperatures.

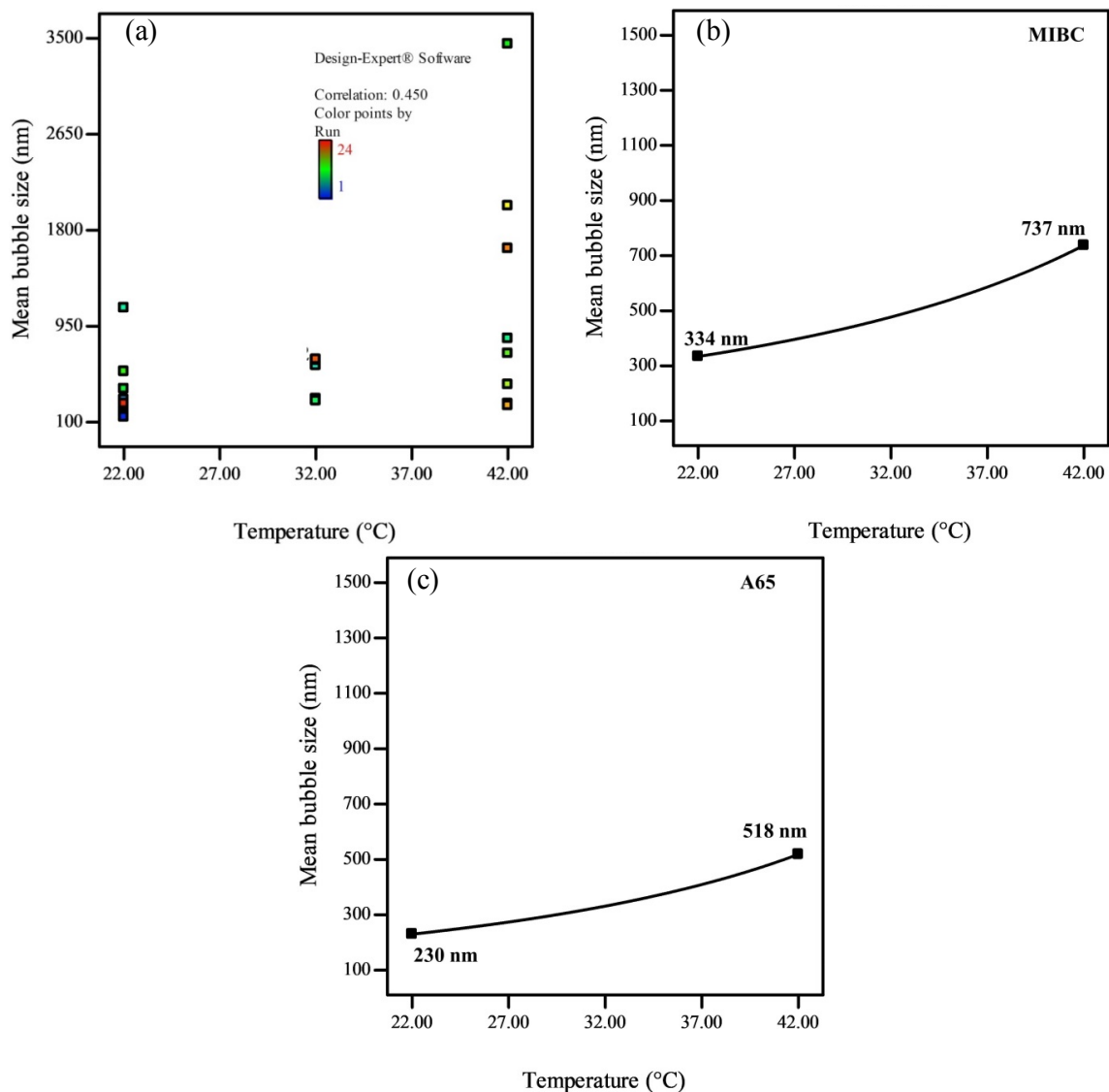


Fig. 9. Mean bubble size as a function of the temperature based on runs (a) and model predictions (b) MIBC and (c) A65 (predictions conditions: pH= 8, frother dosage= 130 mg/L, air flow rate= 0.25 L/min, pressure= 325 kPa)

3.2.4. pH

The effect of pH on the mean bubble size is shown in Fig. 10. As can be seen, the average size of NBs was reduced with increasing pH from 6 to 8 (Fig 10a). It implies that pH 8 creates uniform bubbles with

little size variation. In general, it is clear from the results presented in perturbation graph (Fig. 5) that among factors, pH has the lowest influence on the mean bubble size. Meanwhile, Table A1 and equation A1 demonstrate that pH has no considerable impact on the mean bubble size. Additionally, to obtain a better understanding of pH behavior, we added pH into model and plotted its effect in Fig. 10b and Fig. 10c. As seen, with the increase of pH from 6 to 10, the average size of NBs dropped slightly from 608 to 595 nm for MIBC (Fig 10b) and from 315 to 310 nm for A65 (Fig 10c) under conditions: frother dosage of 90 mg/L, air flow rate of 0.25 L/min, temperature of 32 °C, pressure of 325 kPa. Mostly, it is perceived that OH⁻ group adsorption (because of enthalpy difference in hydration between OH⁻ and H⁺ ions) was dominant at bubbles interface and negative charge of bubble zeta potential in deionized water was determined (Najafi et al., 2007; Elmahdy et al., 2008). By increasing pH, the negative zeta potential of the NBs enhances due to the absorption of OH⁻ ions. The high value of zeta potential creates a surface repulsive force. Other than that, NBs tend to repel each other at high zeta potentials. Increasing bubbles surface charge and electrostatic repulsion force makes smaller bubbles (Wu et al., 2012; Meegoda et al., 2018). Also, the developed electrical double-layer supposedly provides a repulsive force, which prevents inter-bubble aggregation and coalescence (Hamamoto et al., 2018). Recently, Bu et al. (2019) investigated the average size and zeta potential of nanobubbles in different reagent solutions and pH values (2-12). The NBs were generated by dispersing a supersaturated air-water mixture in a mixing chamber, and then causing the breakup of microbubbles in a Teflon hose. The size and zeta potential of the bubbles were measured by dynamic light scattering. They found that the solution pH effect on bubble size was extremely low, however, zeta potential reduced in all solutions, while pH enhanced

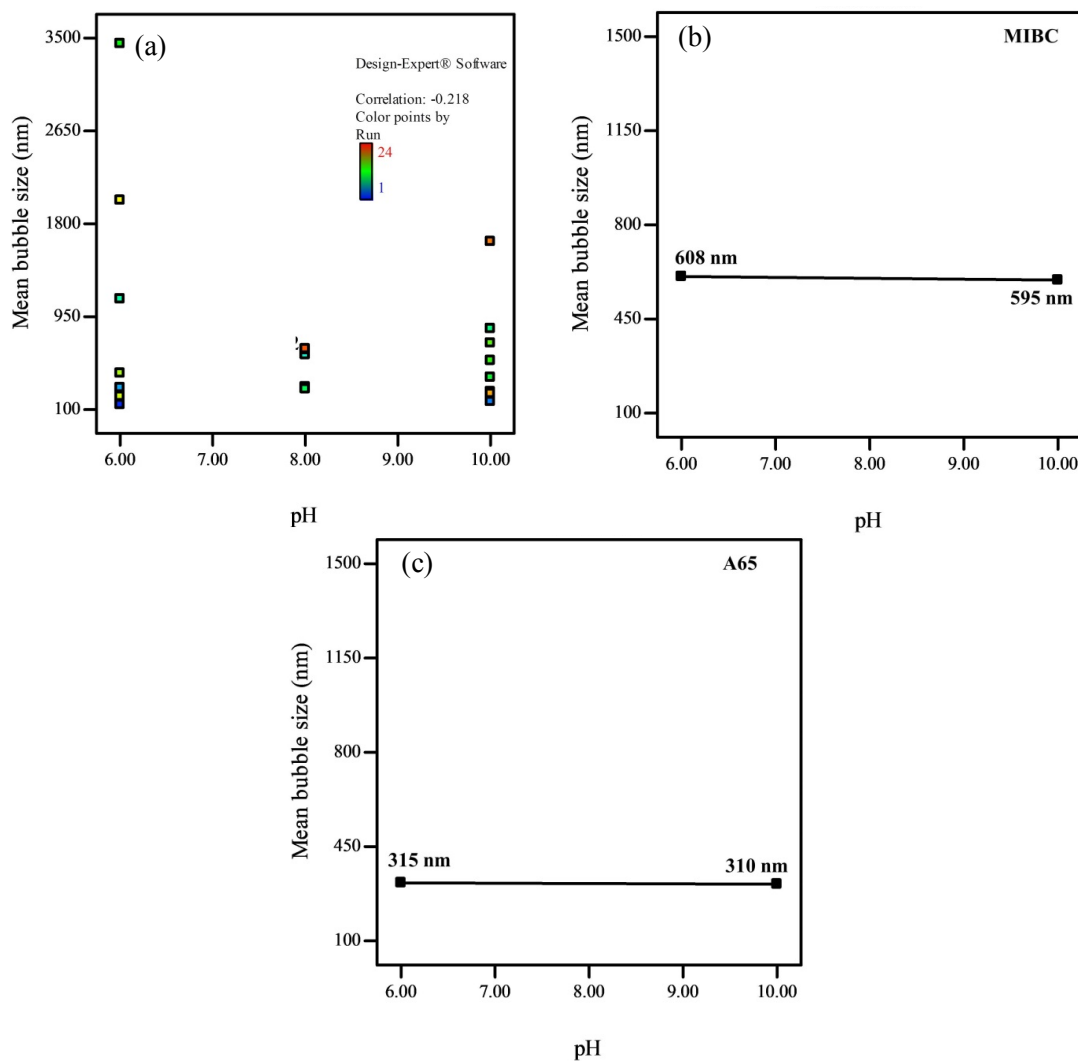


Fig. 10. The impact of pH on the d_{32} based on runs (a) and model predictions (b) MIBC and (c) A65 (prediction conditions: frother dosage= 90 mg/L, air flow rate= 0.25 L/min, temperature= 32 °C, pressure= 325 kPa)

from 2 to 12. The same conclusion was reported by Cho et al. (2005) that bubble size stayed similarly at ~750 nm in the entire pH 2-12. Hamamoto et al. (2018) created the NBs by a pressurized dissolution method while pH of the original water was adjusted to either 5 using HCl (1 mM) or 11 using NaOH (1 mM). It was indicated that the NBs were more stable under higher pH level.

3.2.5. Pressure

The flow rate in Venturi tube is a function of the upstream pressure, the throat area, the density and saturation pressure of the liquid (Brennen, 2014). As can be seen in Fig. 11, the NBs generated by employing high pressure have smaller diameter than those in low pressure. It was found that the bubble size after pressurization was decreased. As a matter of fact, the gas solubility in solution increased with the increase of the pressure and led to the formation of smaller NBs (Wang et al., 2019). Furusaki (2001) observed the effect of pressure on the bubble size distribution. They found that the bubble size was coarser at atmospheric pressure while it became smaller at high temperatures. Bubble formation at gas distributor, bubble coalescence and breakup were effective factors on bubble size. Also, the effect of seawater on bubble size was studied by Johnson and Cooke (1981). They showed that bubbles in seawater contracted when the pressure was increased. Also, bubbles with diameters of 0.75 to 2.25 μm

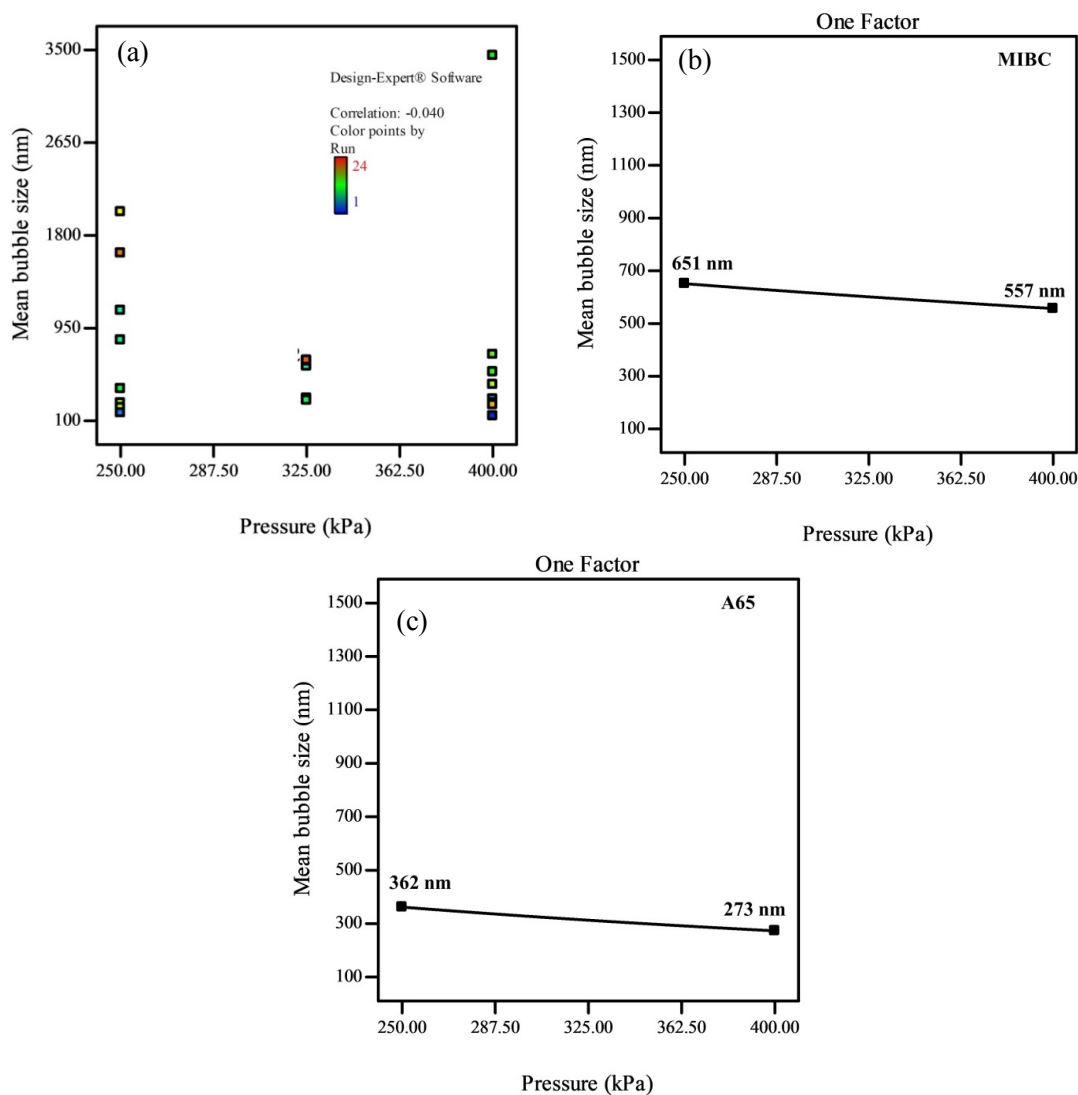


Fig. 11. Obtained bubble Sauter number as a function of pressure drop in Venturi tube based on (a) runs and (b) model predictions using MIBC and (c) A65 (predictions conditions: pH= 8, frother dosage= 90 mg/L, air flow rate= 0.25 L/min, temperature= 32 °C)

were decreased in number by slightly more than one third, while those greater than about 5 μm were reduced by a factor of more than ten. In this study, the bubbles were covered with a surface film of organic surfactants which making them stable. Salt water inhibits coalescence of bubbles and surface area to cause coalescence between bubbles was small. Domnick and Durst (1995) showed the increase in the static pressure at the upstream of the constriction and passed the vena contracta (the point in a fluid stream where the fluid velocity is maximum) at the constriction lead to the smaller bubble, and the number concentration of bubbles decreased with the reduction of static pressure. This result is due to bubble nucleation, growth and coalescence.

3.2.6. Interaction of main factors

In addition to the main effects, the influential parameters interact with each other. Interaction effects indicate that a variable influences the relationship between independent and dependent variables. Studies in the literature yet disregarded the interaction effects of given parameters on nanobubble sizes. Figure 12 depicts the interaction effects between factors. As shown in Equation A1 and Fig. 12, the interaction of AB (frother type and its dosage), AC (frother type and air flow rate) as well as AD (frother type and pressure) are statistically significant on the mean bubble size which is confirmed by p-values (Table A1). According to Fig. 12, different slopes indicate an interaction effect while parallel lines suggest no interaction between the variables. Fig. 12a demonstrates that the relationship between

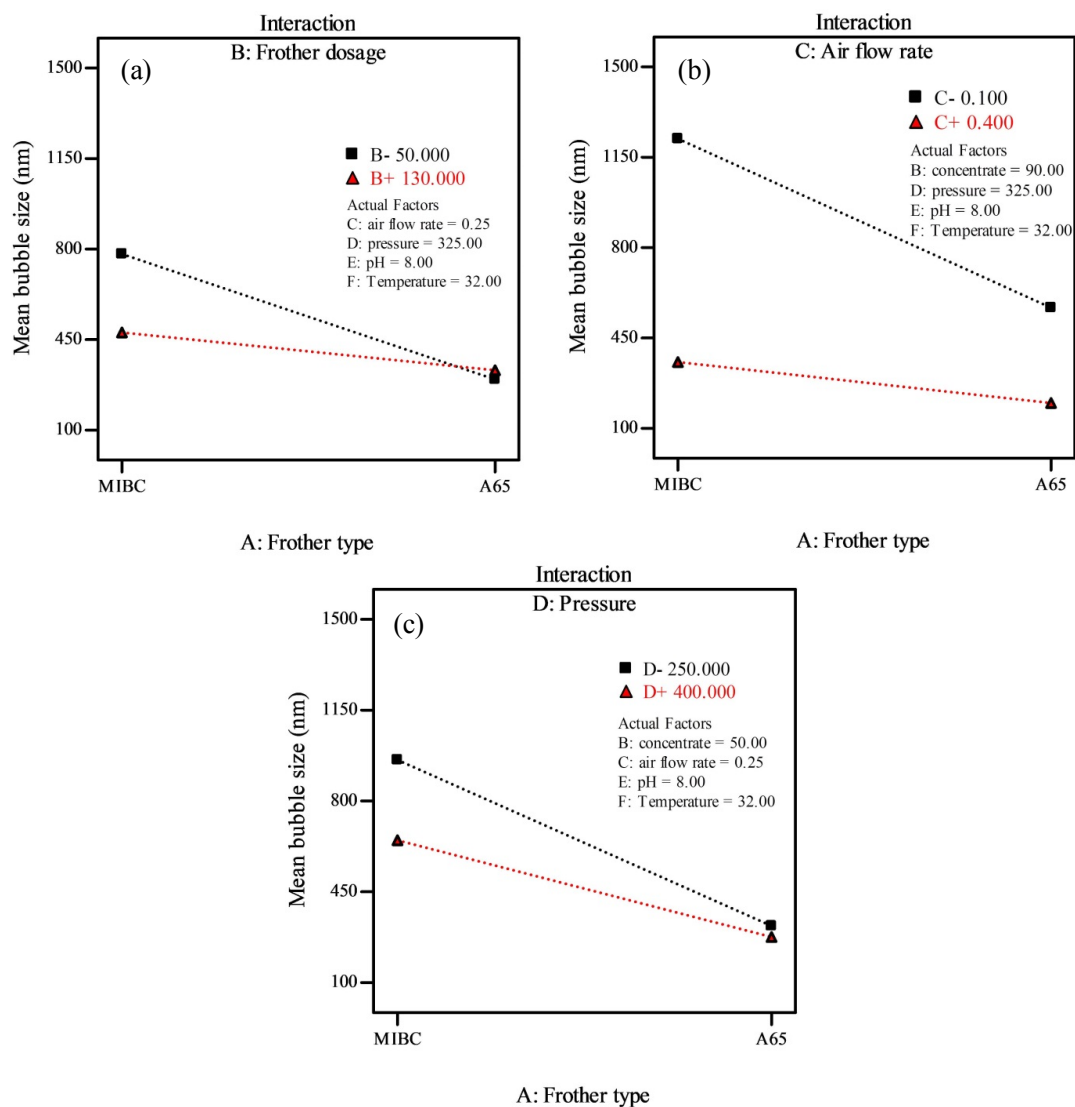


Fig. 12. Interaction plots of two variables a) frother type and frother dosage, b) frother type and air flow rate and c) frother type and pressure

frother type and mean bubble size changes direction based on the frother dosage. For high frother concentrate, there is a positive relationship between frother type and d_{32} . The graph indicates that d_{32} s are larger for A65 when its concentration is 50 mg/L. Fig. 12b displays that when the frother type is MIBC and air flow rate is in high level (0.40 L/min), it results in smaller mean bubble sizes. It can be possibly contributed to coalescence of NBs by increasing the air flow rate. Fig. 12c also exhibits that using A65 either in high or low pressures values does not have significant influence on the d_{32} . However, if the frother type is MIBC, lower pressure induces smaller-sized bubbles. The findings obtained via Han et al., 2002, indicates that the bubble size decreases when the pressure drop increases up to a pressure of 3.5 atmospheres and at higher pressures from this critical value, the bubble size does not reduce. Also, Han et al. (2019) reported that the change in the pressure was resulted in an increase in the turbulence intensity and it caused to an increase in the gas-liquid interaction frequency and consequently d_{32} reduced.

3.3. Flotation experiments

Fig. 13 shows the flotation recovery of coarse-sized quartz particles in the presence of two frother types (MIBC and A65) at the air flow rate of 30 L/h. As can be seen, in case of both frothers and for all fraction sizes, quartz recovery with NBs is higher than that without NBs. The probable reason is that the NBs act like a secondary collector binding coarse particles with coarse bubbles, which ultimately strengthen the buoyancy force of attached-particles to the bubbles (Ahmadi et al., 2014; Nazari et al., 2019).

According to the results, without NB (Fig. 13a), the resultant R_{max} for A65 and MIBC was respectively 61.55% and 76.84%. As presented in Table 5, not only the molecular weight but also the surface tension, and critical coalescence concentration of A65 are greater than MIBC. These properties of A65 result in lowering generated bubble sizes in comparison with the MIBC, which in turn shrinkage the particle-bubble attachment efficiency. Since A65 inherently has higher molecular weight and varies the pulp surface tension more than the MIBC, intensive change of bubble surface zeta potential and its frothability is anticipated. Hence, particles can easily detach from the bubbles due to high surface area of bubbles and coarse size range of particles. In contrast to A65, MIBC produces larger bubbles, which could carry coarse particles. It is also well-known that coarse particles have more affinity to colloid with large bubbles leading to an increase in the particle-bubble collision sub-process (Hassanzadeh et al., 2016). Therefore, a desirable collision and attachment occur between bubbles and particles. Detailed information concerning the effect of particle and bubble sizes on particle-bubble interactions (collision, attachment and stability) of quartz flotation can be found elsewhere (Kouachi et al., 2017).

In the presence of NBs with the air volume content of 0.4 L/min, the R_{∞} for A65 and MIBC was obtained 76.84% and 92.29%, respectively (Fig. 13b). The results presented in Fig. 6a support that A65-NBs are relatively smaller and reasonably uniform than MIBC-NBs, which this statement was recently confirmed by Pourkarimi et al. (2017). Other than bubble size, A65-NBs are more effective on the bubble

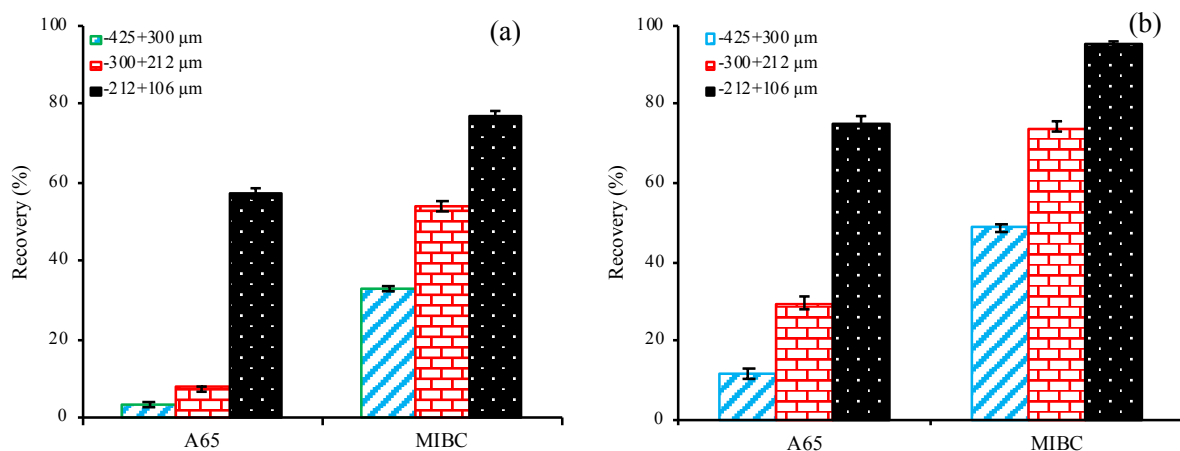


Fig. 13. Recovery of coarse quartz particles using A65 and MIBC a) without NBs and b) with NBs (MIBC and A65= 50 mg/L, DDA= 50 mg/L)

surface charge than the MIBC-NBs, which can be assumed concerning their properties given in Table 5. Increasing the bubble zeta potential increases the surface repulsion forces and thus prevents them from interconnecting and merging (Elmahdy et al., 2008; Ahmadi et al., 2014). This allows the particles attach to the bubbles and recovery increases, as shown in Fig. 13b. So far, zeta potential of A65 and MIBC-NBs remains in the literature as an ongoing argument how the partially-ionized micelles and monomers behave in an equilibrium state in water-bubble and mineral-water interfaces when the NBs are stable in a suspension. Further studies are required for more clarifications.

4. Conclusions

In this research, main and interaction effects of six key parameters were evaluated on BSD of generated NBs using the hydrodynamic cavitation system. For this purpose, well-known fractional factorial-based design (2^{6-2}) was utilized. Frother type (MIBC and A65), frother dosage (50, 90 and 130 mg/L), air flow rate (0.1, 0.25 and 0.40 L/min), pressure in the Venturi tube (250, 325 and 400 kPa), liquid temperature (22, 32 and 42 °C) and pH (6, 8 and 10) were variable and the Sauter mean diameter was considered as the response. Finally, flotation of coarse-sized quartz particles with and without NBs in a laboratory mechanical flotation cell was examined.

The experimental results indicated that three parameters critically influenced on d_{32} of NBs which could be orderly sorted as air flow rate > temperature > frother type. Using A65 statistically produced significant smaller bubbles than the MIBC. By rising the temperature from 22 °C to 42 °C, the bubble size increased. Temperature induced formation of bubbles at a lower liquid flow velocity in the Venturi tube, which was due to an increase in water vapor pressure and, consequently, a reduction in the number of cavitation. Also, growing the temperature increased the density of bubbles. Furthermore, by changing the air flow rate from 0.1 to 0.4 L/min, the amount of dissolved gas in the solution was enhanced, which led to decreasing the concentration of gas at the interface of the gas-liquid which improved stability of the NBs and resulted in smaller mean bubble sizes. Thus, it was concluded that the smaller bubbles were generated with the increase in air flow rate for both types of frother, but generated bubbles by the A65 were smaller than the MIBC. It was also found that alkaline pH was favorable for producing smaller-sized NBs mainly owing to greater adsorption of the OH⁻ group and its effect on negatively charging the bubble surfaces. Eventually, the comparative results obtained from the flotation experiments in the presence and absence of NBs indicated that the recovery of coarse particles was up to 22% excessive than that in the absence of NBs.

Acknowledgment

The authors would like to thank University of Tehran and the Iran Mineral Processing Research Center (IMPRC) for financially supporting this research work. The third author also intends to express his appreciation to Helmholtz Institute Freiberg for Resource Technology (Germany) for supporting this research. We would like to thank anonymous reviewers for their insightful remarks, constructive comments and fruitful criticisms.

Nomenclature

NBs	Nanobubbles	R	Flotation recovery (%)
CBs	Conventional bubbles	C	Concentrate mass (g)
MIBC	Methyl isobutyl carbinol	F	Feed mass (g)
A65	Polypropylene glycol	d_{32}	Sauter mean diameter
ANOVA	Analysis of variance	BSD	Bubble size distribution

Appendix

Appendix A: The given ANOVA tabulated for the studied fractional design according to the Equation A1.

$$1/\sqrt{d_{32}} = 0.049 + 0.00788 \times A + 0.0017 \times B + 0.013 \times C + 0.00279 \times D - 0.00998 \times F - 0.0033 \times A \times B + 0.00119 \times A \times C + 0.00119 \times A \times D + 0.00189 \times A \times B \times D - 0.00103 \times A \times B \times F \quad (A1)$$

$$R^2 = 0.9986, \text{ Adj } R^2 = 0.9975$$

where d_{32} is average diameter (nm), A is the frother type, B is the frother concentrate, C is the air flow rate, D is the pressure, E is the pH and F is the temperature. Also, $A \times B$ is the interaction effect of frother type and frother concentrate, $A \times C$ denotes the interaction effect between frother type and air flow rate and $A \times D$ shows influential effect of frother type and pressure.

Table A1. ANOVA for the factorial factorial model

Source	Sum of squares	Df*	Mean square	F-value	p-value Prob>F
Model	6.57E-03	10	6.57E-04	935.39	< 0.0001
A: Frother type	9.94E-04	1	9.94E-04	1414.18	< 0.0001
B: Frother concentrate	4.60E-05	1	4.60E-05	65.41	< 0.0001
C: Air flow rate	2.86E-03	1	2.86E-03	4063.7	< 0.0001
D: Pressure	1.24E-04	1	1.24E-04	176.67	< 0.0001
F: Temperature	1.59E-03	1	1.59E-03	2267.83	< 0.0001
AB	1.74E-04	1	1.74E-04	247.95	< 0.0001
AC	2.25E-05	1	2.25E-05	32.04	< 0.0001
AD	2.27E-05	1	2.27E-05	32.25	< 0.0001
ABD	5.70E-05	1	5.70E-05	81.05	< 0.0001
ABF	1.70E-05	1	1.70E-05	24.26	0.0003
Residual	9.13E-06	13	7.03E-07		
Lack of fit	4.98E-06	7	7.11E-07	1.03	0.496
Pure error	4.16E-06	6	6.93E-07		

*DF – degrees of freedom

References

- AGARWAL, A., NG, W.J., LIU, Y., 2011. *Principle and applications of microbubble and nanobubble technology for water treatment*. Chemosphere. 84, 1175-1180. DOI: 10.1016/j.chemosphere.2011.05.054
- AHMADI, R., KHODADADI DARBAN, A., 2013. *Modeling and optimization of nano-bubble generation process using response surface methodology*. International Journal of Nanoscience and Nanotechnology. 9, 151-162.
- AHMADI, R., DARBAN, A.K., ABDOLLAHY, M., FAN, M., 2014. *Nano-microbubble flotation of fine and ultrafine chalcopyrite particles*. Int. J. Min. Sci. Technol. 24, 559-566. DOI: 10.1016/j.ijmst.2014.05.021
- ARIAS, S., RUIZ, X., CASADEMUNT, J., 2009. *Experimental study of a microchannel bubble injector for microgravity applications*. Microgravity Sci. Technol. 21, 107-111. DOI 10.1007/s12217-008-9060-1
- AZEVEDO, A., ETCHEPARE, R., CALGAROTO, S., RUBIO, J., 2016. *Aqueous dispersions of nanobubbles: Generation, properties and features*. Miner. Eng. 94, 29-37. DOI: 10.1016/j.mineng.2016.05.001
- AZEVEDO, A., ETCHEPARE, R., RUBIO, J., 2017. *Raw water clarification by flotation with microbubbles and nanobubbles generated with a multiphase pump*. Water Sci. Technol. 75, 2342-2349. DOI: 10.2166/wst.2017.113
- AZIZI, A., MASDARIAN, M., HASSANZADEH, A., BAHRI, Z., NIEDOBA, T., SUROWIAK, A., 2020. *Parametric optimization in rougher flotation performance of a sulfidized mixed copper ore*, Minerals. 10(8), 660, 1-19. DOI: 10.3390/min10080660
- KATAL, R., AZIZI, A., GHARABAGHI, M., 2020. *Investigating the leaching behavior of copper from chalcopyrite concentrate in H₂SO₄/CuCl₂ Media*. IJMSE. 17(2), 66-76. DOI: 10.22068/ijmse.17.1.66
- BRENNEN, C.E., 2014. *Cavitation and bubble dynamics*. Cambridge University Press. First published.
- BU, T.T., NGUYEN, D.C., HAN, M., 2019. *Average size and zeta potential of nanobubbles in different reagent solutions*. J. Nanopart. Res. 21, 173.
- CALGAROTO, S., AZEVEDO, A., RUBIO, J., 2015. *Flotation of quartz particles assisted by nanobubbles*. Int. J. Miner. Process. 137, 64-70. DOI: 10.1016/j.minpro.2015.02.010.
- CHEN, Q., WIEDENROTH, H. S., GERMAN, S. R., WHITE, H. S., 2015. *Electrochemical Nucleation of Stable N₂ Nanobubbles at Pt Nanoelectrodes*. J. Am. Chem. Soc. 137, 12064-12069. DOI: 10.1021/jacs.5b07147

- CHO, S-H., KIM, J-Y., CHUN, J-H., KIM, J-D., 2005. *Ultrasonic formation of nanobubbles and their zeta-potentials in aqueous electrolyte and surfactant solutions*. Colloids Surf. A Physicochem. Eng. Asp. 269, 28-34. <https://doi.org/10.1016/j.colsurfa.2005.06.063>
- DOMNICK, J., DURST, F., 1995. *Measurement of bubble size, velocity and concentration in flashing flow behind a sudden constriction*. Int. J. Multiph. Flow. 21, 1047-1062. DOI: 10.1016/0301-9322(95)00045-Y
- DUONG, H.H., HASSANZADEH, A., PEUKER, U.A., RUDOLPH, M., 2019. *Impact of flotation hydrodynamics on the optimization of fine-grained carbonaceous sedimentary apatite ore beneficiation*. Powder Technol. 345, 223-233. <https://doi.org/10.1016/j.powtec.2019.01.014>
- ELMAHDY, A.M., MIRNEZAMI, M., FINCH, J. A., 2008. *Zeta potential of air bubbles in presence of frothers*. Int. J. Miner. Process. 89, 40-43. DOI: 10.1016/j.minpro.2008.09.003
- FAN, M., ZHAO, Y., TAO, D., 2012. *Fundamental studies of nanobubble generation and applications in flotation*. Separation Technologies for Minerals, Coal, and Earth Resources, Society for Mining, Metallurgy, and Exploration, Littleton, CO. 457-469.
- FAN, M., TAO, D., 2008. *A study on picobubble enhanced coarse phosphate froth flotation*. Sep. Sci. Technol. 43, 1-10. DOI: 10.1080/01496390701747853
- FAN, M., TAO, D., HONAKER, R., LUO, Z. F., 2010. *Nanobubble generation and its application in froth flotation (part I): nanobubble generation and its effects on properties of microbubble and millimeter scale bubble solutions*. Min. Sci. Technol. 20, 1-19. DOI: 10.1016/S1674-5264(09)60154-X
- FAN, M., TAO, D., HONAKER, R., LUO, Z. F., 2010. *Nanobubble generation and its applications in froth flotation (part III): specially designed laboratory scale column flotation of phosphate*. Int. J. Min. Sci. Technol. 20, 317-338. DOI: 10.1016/S1674-5264(09)60205-2
- FAN, M., TAO, D., HONAKER, R., LUO, Z. F., 2010. *Nanobubble generation and its applications in froth flotation (part IV): mechanical cells and specially designed column flotation of coal*. Min. Sci. Technol. 20, 641-671. DOI: 10.1016/S1674-5264(09)60259-3
- FARMER, A., COLLINGS, A., JAMESON, G., 2000. *Effect of ultrasound on surface cleaning of silica particles*. Int. J. Miner. Process. 60, 101-113. DOI: 10.1016/S0301-7516(00)00009-0
- FURUSAKI, S., 2001. *The expanding world of chemical engineering*. CRC Press. 175-176.
- GUVEN, O., BATJARGAL, K., OZDEMIR, O., KARAKASHEV, S.I., GROZEV, N.A., BOYLU, F., ÇELIK, M.S., 2020. *Experimental procedure for the determination of the critical coalescence concentration (CCC) of simple frothers*, 10. 617, 1-12. DOI:10.3390/min10070617
- HAMAMOTO, S., TAKEMURA, T., SUZUKI, K., NISHIMURA, T., 2018. *Effects of pH on nano-bubble stability and transport in saturated porous media*. J. Contam. Hydrol. 208, 61-67. DOI: 10.1016/j.jconhyd.2017.12.001
- HAMPTON, M., NGUYEN, A., 2010. *Nanobubbles and the nanobubble bridging capillary force*. Adv. Colloid Interface Sci. 154, 30-55. DOI: 10.1016/j.cis.2010.01.006
- HAN, M., PARK, Y., LEE, J., SHIM, J., 2002. *Effect of pressure on bubble size in dissolved air flotation*. Water. Supply. 2(5-6): 41-46. DOI: 10.2166/ws.2002.0148
- HAN, Y., ZHU, J., SHEN, L., ZHOU, W., LING, Y., YANG, X., WANG, S., DONG, Q., 2019. *Bubble Size Distribution Characteristics of a Jet-Stirring Coupling Flotation Device*. Minerals. 9(6), 369. DOI: 10.3390/min9060369
- HASSANZADEH, A., VAZIRI HASSAS, B., KOUACHI, S., BRANCOVA, Z., CELIK, M.S., 2016. *Effect of bubble size and velocity on collision efficiency in chalcopyrite flotation*. Colloids Surf. A Physicochem. Eng. Asp. 498, 258-267. [https://doi.org/10.1016/0301-9322\(95\)00045-Y](https://doi.org/10.1016/0301-9322(95)00045-Y)
- HASSANZADEH, A., KOUACHI, S., HASANZADEH, M., CELIK, M.S., 2017. *A new insight to the role of bubble properties on inertial effect in particle-bubble interaction*. J. Dispers. Sci. Technol. 38, 953-960. <https://doi.org/10.1080/01932691.2016.1216437>
- HASSANZADEH, A., KARAKAS, F., 2017. *Recovery improvement of coarse particles by stage addition of reagents in industrial copper flotation circuit*. J. Dispers. Sci. Technol. 38, 309-316. <https://doi.org/10.1080/01932691.2016.1164061>
- HASSANZADEH, A., FIROUZI, M., ALBIJANIC, B., CELIK, M.S., 2018. *A review on determination of particle-bubble encounter using analytical, experimental and numerical methods*. Miner. Eng. 122, 296-311. <https://doi.org/10.1016/j.mineng.2018.04.014>
- HASSANZADEH, A., AZIZI, A., KOUACHI, S., KARIMI, M., CELIK, M.S., 2019. *Estimation of flotation rate constant and particle-bubble interactions considering key hydrodynamic parameters and their interrelations*. Miner. Eng. 141, 105836. <https://doi.org/10.1016/j.mineng.2019.105836>

- HASSANZADEH, A., SAJJADY, S.A., GHOLAMI, H., AMINI, S., ÖZKAN, S.G., 2020. *An improvement on selective separation by applying ultrasound to rougher and re-cleaner stages of copper flotation*, Minerals, 10(7), 619, 1-19. <https://doi.org/10.3390/min10070619>
- JOHNSON, B.D., COOKE, R.C., 1981. *Generation of stabilized microbubbles in seawater*. Sci. 213, 209-211. DOI: 10.1126/science.213.4504.209
- KIM, J. Y., SONG, M. G., KIM, J. D., 2000. *Zeta potential of nanobubbles generated by ultrasonication in aqueous alkyl polyglycoside solutions*. J. Colloid Interface Sci. 223, 285-291. DOI: 10.1006/jcis.1999.6663
- KOUACHI, S., VAZIRI HASSAS, B., HASSANZADEH, A., CELIK, M.S., BOUHENGUEL, M., 2017. *Effect of negative inertial forces on bubble-particle collision via implementation of Schulze collision efficiency in general flotation rate constant equation*. Colloids Surf. A Physicochem. Eng. Asp. 517, 72-83. <https://doi.org/10.1016/j.colsurfa.2017.01.002>
- KRACHT, W., MORAGA, C., 2016. *Acoustic measurement of the bubble Sauter mean diameter d32*. Miner. Eng. 98, 122-126. DOI: 10.1016/j.mineng.2016.08.001
- KUMAR, R., KENTISH, S., ASHOKKUMAR, M., 2009. *Selected applications of ultrasonic in food processing*, Raman Kumar Bhaskaracharya, Food Eng. Rev. 1, 31-49. DOI: 10.1007/s12393-009-9003-7
- LEI, W., ZHANG, M., ZHANG, Z., ZHAN, N., FAN, R., 2020. *Effect of bulk nanobubbles on the entrainment of kaolinite particles in flotation*. Powder Technol. 362, 84-89. DOI: <https://doi.org/10.1016/j.powtec.2019.12.015>
- LOU, S. T., OUYANG, Z. Q., ZHANG, Y., 2000. *Nanobubbles on solid surface imaged by atomic force microscopy*. Journal of Vacuum Science & Technology B: Microelectronics and Nanometer Structures Processing. Measurement, and Phenomena. 18, 2573-2575. DOI: 10.1116/1.1289925
- MEEGODA, N., ALUTHGUN HEWAGE, S., BATAGODA, J.H., 2018. *Stability of nanobubbles*. Environ. Eng. Sci. 35, 1216-1227. DOI: 10.1089/ees.2018.0203
- NAJAFI, A., DRELICH, J., YEUNG, A., XU, Z., MASLIYAH, J., 2007. *A novel method of measuring electrophoretic mobility of gas bubbles*. J. Colloid Interface Sci. 308, 344-350. DOI: 10.1016/j.jcis.2007.01.014
- NAZARI, S., SHAFAEI, S.Z., SHAHBAZI, B., CHEHREH CHELGANI, S., 2018. *Study relationships between flotation variables and recovery of coarse particles in the absence and presence of nanobubble*. Colloids Surf. A Physicochem. Eng. Asp. 559, 284-289. DOI: 10.1016/j.colsurfa.2018.09.066.
- NAZARI, S., SHAFAEI, S.Z., GHARABAGHI, M., AHMADI, R., SHAHBAZI, B., 2018. *Effect of frother type and operational parameters on nano bubble flotation of quartz coarse particles*. Journal of Mining & Environment. 9, 539-546. DOI: 10.22044/jme.2017.6404.1461
- NAZARI, S., SHAFAEI, S.Z., GHARABAGHI, M., AHMADI, R., SHAHBAZI, B., TEHRANCHI, A., 2018. *New approach to quartz coarse particles flotation using NBs, emphasis on the bubble size distribution*. Int. J. Nanosci. 19. DOI: 10.1142/S0219581X18500485.
- NAZARI, S., SHAFAEI, S.Z., GHARABAGHI, M., AHMADI, R., SHABAZI, B., FAN, M., 2019. *Effects of nanobubble and hydrodynamic parameters on coarse quartz flotation*. Int. J. Min. Sci. Technol. 29, 289-295. DOI: 10.1016/j.ijmst.2018.08.011.
- NAZARI, S., CHEHREH CHELGANI, S., SHAFAEI, S.Z., SHAHBAZI, B., SOLIMANI MATIN, S., GHARABAGHI, M., 2019. *Flotation of coarse particles by hydrodynamic cavitation generated in the presence of conventional reagents*. Sep. Purif. Technol. 220, 61-68. DOI: 10.1016/j.seppur.2019.03.033
- NAZARI, S., HASSANZADEH, A., 2020. *The effect of reagent type on generating bulk sub-micron (nano) bubbles and flotation kinetics of coarse-sized quartz particles*, Powder Technol. 374, 160-171. <https://doi.org/10.1016/j.powtec.2020.07.049>
- NEETHIRAJAN, S., KOBAYASHI, I., NAKAJIMA, M., WU, D., NANDAGOPAL, S., LIN, F., 2011. *Microfluidics for food, agriculture and biosystems industries*. Lab Chip. 11, 1574-1586.
- NIRMALKAR, N., PACEK, A. W., BARIGOU, M., 2018. *Interpreting the Interfacial and Colloidal Stability of Bulk Nanobubbles*. Soft Matter. 14, 9643-9656. DOI: 10.1039/C8SM01949E
- PAXTON, W.F., C. KISTLER, K., C. OLMEDA, C., SEN, A., K. ST. ANGELO, S., CAO, Y., E. MALLOUK, T., E. LAMMERT, P., H. CRESPI, V., 2004. *Catalytic nanomotors: autonomous movement of striped nanorods*. J. Am. Chem. Soc., 126, 13424-13431. DOI: 10.1021/ja047697z
- POURKARIMI, Z., REZAI, B., NOAPARAST, M., 2017. *Effective parameters on generation of nanobubbles by cavitation method for froth flotation applications*. Physicochem. Probl. Miner. Process. 53, 920-942. DOI: 10.5277/ppmp170220
- RATH, S.S., SAHOO, H., DAS, B., 2013. *Optimization of flotation variables for the recovery of hematite particles from BHQ ore*. Int. J. Miner. Metall. Mater. 20, 605-611. DOI: 10.1016/j.cjche.2018.02.014

- RULYOV, N.N., FILIPPOV, L.O., KRAVCHENKO, O.V., 2020. *Combined microflotation of glass beads*, *Colloids Surf. A Physicochem. Eng. Asp.* 598, 124810. <https://doi.org/10.1016/j.colsurfa.2020.124810>
- SHAHBAZI, B., 2015. *Study of relationship between flotation rate and bubble surface area flux using bubble-particle attachment efficiency*. *Am. J. Chem. Eng.* 3, 6-12. DOI: 10.11648/j.ajche.s.2015030202.12
- TAO, D., SOBHY, A., 2019. *Nanobubble effects on hydrodynamic interactions between particles and bubbles*. *Powder Technol.* 346, 385-395. DOI: 10.1016/j.powtec.2019.02.024
- WANG, Q., ZHAO, H., QI, N., QIN, Y., ZHANG, X., LI, Y., 2019. *Generation and stability of size-adjustable bulk nanobubbles based on periodic pressure change*, *Sci. Rep. (Nature Publisher Group); London.* 9, 1118. DOI: 10.1038/s41598-018-38066-5
- WU, C., NESSET, K., MASLIYAH, J., XU, Z., 2012. *Generation and characterization of submicron size bubbles*. *Adv. Colloid Interface Sci.* 179-182, 123-132.
- XIAO, W., ZHAO, Y., YANG, J., REN, Y., YANG, W., HUANG, X., ZHANG, L., 2019. *Effect of sodium oleate on the adsorption morphology and mechanism of nanobubbles on the mica surface*. *Langmuir.* 35, 9239-9245. DOI: 10.1021/acs.langmuir.9b01384
- YEKEEN, N., IDRIS, K. A., A. MANAN, M., SAMIN, A. M., RISAL, A.R., XIN KUN, T., 2017. *Bulk and bubble-scale experimental studies of influence of nanoparticles on foam stability*. *Chin. J. Chem. Eng.* 25, 347-357. DOI: 10.1016/j.cjche.2016.08.012
- ZHANG, X., WANG, Q.S., WU, Z.X., TAO, D.P., 2020. *An experimental study on size distribution and zeta potential of bulk cavitation nanobubbles*. *Int. J. Miner. Metall. Mater.* 27, 152-161. DOI: 10.1007/s12613-019-1936-0
- ZHANG, X.H., KHAN, A., DUCKER, W. A., 2007. *A nanoscale gas state*. *Phys. Rev. Lett.* 98, 136101. DOI: 10.1103/PhysRevLett.98.136101
- ZHANG, X.H., LI, G., WU, Z.H., ZHANG, X.D., HU, J., 2005. *Effect of temperature on the morphology of nanobubbles at mica/water interface*. *Chinese Phys.* 14, 1774-1778. DOI: 10.1088/1009-1963/14/9/015/meta
- ZHOU, Z. A., XU, Z., FINCH, J. A., HU, H., RAO, S. R., 1997. *Role of hydrodynamic cavitation in fine particle flotation*. *Int. J. Miner. Process.* 51, 139-149. DOI: 10.1016/S0301-7516(97)00026-4